Materials & Design 241 (2024) 112882

Contents lists available at ScienceDirect

Materials & Design

journal homepage: www.elsevier.com/locate/matdes

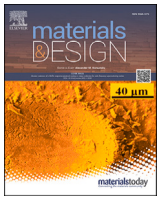

On the influence of low-velocity impact damage on constrained-layer damping in hybrid CFRP-elastomer-metal laminates

Alexander Jackstadt [a,*], Wilfried V. Liebig [b], Kay A. Weidenmann [c], Luise Kärger [a]

[a] Karlsruhe Institute of Technology (KIT), Institute of Vehicle System Technology - Lightweight Engineering, Rintheimer Querallee 2, Karlsruhe, 76131, Baden-Württemberg, Germany
[b] Karlsruhe Institute of Technology (KIT), Institute for Applied Materials - Materials Science and Engineering, Engelbert-Arnold-Straße 4, Karlsruhe, 76131, Baden-Württemberg, Germany
[c] University of Augsburg, Institute of Materials Resource Management - Hybrid Composite Materials, Am Technologiezentrum 8, Augsburg, 86159, Bavaria, Germany

ARTICLE INFO

Keywords:
Fiber metal laminates
Vibration
Damping
Viscoelasticity
Elastomers
Finite element simulation

ABSTRACT

Following the principle of constrained-layer damping (CLD), fiber-metal-elastomer laminates (FMELs) offer a high potential for damped lightweight structures, overcoming the undesirable vibration characteristics of conventional lightweight materials. While proven to be versatile and efficient, the damage-tolerance of such laminates is unexplored. This study for the first time in literature addresses the damage-tolerance of this efficient damping mechanism using a combined experimental and numerical approach. Results of experimental low-velocity impact tests on different configurations of FMELs are presented. In subsequent numerical modal analyses, different types of damage, namely delaminations, intra-ply damage and permanent deformation, are modeled and their influence on the vibrational behavior is investigated. While all types of damage influence the natural frequencies and modal damping ratios with a strong mode dependency, all laminates retain a high amount of modal damping with losses typically not higher than 15%. The results obtained reveal, that CLD is an efficient intrinsic damping measure in FMELs even in the presence of different types of damage. The key contributions of this paper include the thorough experimental characterization of low-velocity impact damages in different configurations of FMELs as well as the numerical assessment of those in frequency-domain simulations.

1. Introduction

1.1. Motivation

The mechanical behavior of fiber-metal laminates (FMLs), such as glass fiber reinforced aluminum, has over the last decades attracted great interest from both, academia and industry. Among other properties, their superior fatigue and impact resistance [1,2] allowed for a wide range of structural applications, especially in the aerospace sector [3]. A replacement of the glass fiber-reinforced polymer (GFRP) plies by carbon fiber-reinforced polymer (CFRP) can significantly improve the mechanical properties such as stiffness and strength, but leads to corrosion problems in the interface with aluminum and residual stresses due to a mismatch in thermal expansion coefficients. The use of elastomeric plies in these interfaces not only resolves these issues [4], but provides versatile options of increasing and optimizing the vibration damping capabilities of FMLs by means of constrained-layer damping (CLD) [5], where under bending loads the highly compliant viscoelastic elastomer plies undergo high transverse shear deformations allowing for significant dissipation of vibration energy [6]. The damping behavior of these hybrid CFRP-elastomer-metal laminates (HyCEMLs) has been studied in detail [7–9], highlighting the versatility and adaptability of the CLD mechanism in hybrid laminates. While there is some recent research on the impact behavior of HyCEML [10] and similar FMELs with varying constituents [11–13], the authors are not aware of any work on the specific damage tolerance of the CLD mechanism in lightweight design. Therefore, this work aims at the analysis of the influence of low-velocity impact damage on the damping capabilities of HyCEML using experimental and numerical methods.

1.2. Related research

Numerous publications deal with the impact behavior of conventional FMLs, in which experimental, analytical and numerical methods

* Corresponding author.
E-mail address: alexander.jackstadt@kit.edu (A. Jackstadt).

https://doi.org/10.1016/j.matdes.2024.112882
Received 30 October 2023; Received in revised form 5 March 2024; Accepted 24 March 2024
Available online 29 March 2024

are applied. Since the mechanical response of such laminates under low-velocity impact loading is well understood, a thorough review of the relating literature is omitted for brevity. Instead, the reader is referred to comprehensive review papers by Sadighi et al. [2], Sinmazçelik et al. [1] and He et al. [14] regarding this subject. The state of the art in impact behavior of FMEL, however, is summarized in greater detail, beginning with Sarlin et al. [15,16], who describe the effect of impact energy and rubber thickness on the high velocity impact properties of hybrid laminates containing steel, elastomer and glass fiber reinforced epoxy. The authors show that the addition of elastomer significantly reduces the interfacial and internal damage in the structure. The total amount of energy absorbed, however, does not change. The area of damage is found to be linearly dependent on the impact energy. The main damage mechanisms were identified to be delamination in interfaces with rubber, as well as fiber matrix debonding. Düring et al. [17] investigate a similar material system consisting of CFRP and GFRP as well as steel plies and an ethylene propylene diene (EPDM) based elastomer. The elastomer, however, is not situated in the interface between the fiber-reinforced polymer (FRP) and steel but between FRP plies. The authors conduct low-velocity impact tests in order to determine the influence of different steel ply thicknesses and the addition of a rubber ply on internal and external damage, the absorbed energy, force evolution, and deformation. They conclude that the addition of a rubber ply increases the damage threshold, below which the structure's response to impact is dominated by global elastic deformation and decreased internal and external damage. In another publication, Düring et al. [11] complement their previous studies by investigating the impact response and damage resistance of additional laminates containing two elastomer plies instead of one. They found that the additional ply leads to a significantly smaller delamination area, as well as minimizing the internal damage resulting from low-velocity impact loading. Li et al. [10] numerically investigate the low-velocity impact behavior of HyCEMLs as considered in the current study. They determine how the introduction of an elastomeric interply influences the damage evolution during impact events compared to conventional FMLs without elastomer plies. Similar conclusions to [11] are reached, namely a significant reduction of damaged areas after the introduction of elastomeric interlayers. FMEL containing GFRP, aluminum and natural rubber are investigated regarding low-velocity impact by Zarezadeh-Mehrizi [12], who give insight into the optimal position of rubber plies within the laminate for minimal damage. Mahesh [13], similar to [10], find that the introduction of elastomer plies in thermoplastic FMEL alter the load distribution during low-velocity impact events, thus causing a wider participation of material in the load bearing process.

The vibration characteristics of undamaged HyCEMLs have been studied experimentally by Sessner et al. [5,8,9] and are complemented by simulations in [18,7], highlighting the influence of numerous lamination schemes as well as temperature and loading conditions. A comprehensive analytical modeling approach for vibrating heterogeneous laminates has been developed by Jackstadt et al. [19–21].

The vibrational behavior of damaged FRP structures has first been modeled by Ramkumar et al. [22], Wang et al. [23] and Mujumdar and Suryanarayan [24]. Better agreement with experimental results are reported by Shen and Grady [25], who analyze the free vibration of delaminated beams using an analytical sublaminate model based on Timoshenko beams, overcoming the previous neglection of shear deformations. Their modeling approach allows for open as well as constrained delamination, depending on whether the crack is allowed to open freely or is kinematically coupled with the other sublaminate. Numerous publications dealing with free vibration of delaminated beams follow up on this approach of open and constrained delaminations, including, but not limited to [26–30]. Further work on delaminated beams includes the consideration of nonlinear effects by Luo and Hanagud [31]. Curved beams with delaminations are addressed by Jafari-Talookolaei [32]. There is additional research on free vibration of delaminated composite beams, most of which is also summarized by Della and Shu [33].

Table 1
Linear elastic material parameters of CFRP under the assumption of transverse isotropy. G_{23} not determined experimentally, but calculated based on assumptions.

E_1 in GPa	E_2 in GPa	ν_{12}	G_{12} in GPa	G_{23} in GPa
103.10	7.7	0.34	3.76	2.75

Table 2
Mechanical properties of aluminum wrought alloy EN AW-2024 T3 ALCLAD AMS-QQA-250/5. Values taken from [18].

Property	Unit	Value
Mass density	$\mathrm{kg\,m^{-3}}$	2770
Young's modulus E	GPa	73.1
Poisson's ratio ν	-	0.3

Yin and Jane [34] find that for delaminated plates, open delaminations modeled with an unconstrained approach lead to additional vibration modes, which is confirmed by Chen [35]. Further works apply the finite element method (FEM) [36,37] or perturbation methods [38] to determine the vibration characteristics of delaminated plates and shells.

Most of the research on vibration of damaged laminates is limited to conventional composite materials. To the authors' knowledge, only Li et al. [39] have investigated the influence of low-velocity impact damage on the vibrational characteristics of FMEL. They present an analytical model and assume a stiffness degradation summarizing all types of occurring damage in a circular area around the point of impact.

This study presents a thorough investigation on the influence of impact damage on CLD in HyCEMLs with a differentiation of type and extent of damage, which makes the results presented here a novelty within research on FMELs. In contrast to previous works on HyCEMLs investigating its damping behavior [40,21] or impact resistance [10], this paper's focus lies on the materials' tolerance to damage with regard to its damping capabilities. Different laminate layups and choices of viscoelastic material for the damping plies are investigated.

2. Materials and methods

2.1. HyCEML

The HyCEMLs investigated in this work consist of three individual constituents, namely CFRP, aluminum and an elastomeric damping material. CFRP plies consist of cured unidirectionally reinforced epoxy-based prepreg sheets HexPly M77/38/UD150/CHS-12K-70 by Hexcel with the linear elastic properties listed in Table 1. The cured CFRP plies have a nominal thickness of 0.15 mm.

The aluminum plies are EN AW-2024 T3 ALCLAD AMS-QQA-250/5 alloy sheets with a thickness of 0.3 mm. Their linear elastic properties and mass density are shown in Table 2.

For the elastomeric viscoelastic damping plies embedded within HyCEML, two different materials are investigated. Both EPDM based elastomers are from the KRAIBON® range of products supplied by Gummiwerk KRAIBURG GmbH & Co. KG, namely SAA9579/52 and HAA9275/45. The former will be abbreviated as E1 in this study, whereas the latter will be denoted as E2. Their mass densities and Shore hardness are shown in Table 3.

The mechanical behavior of the two elastomers, expressed by the complex modulus approach

$$E^* = E' + \mathrm{i}E'' = E'\,(1 + \mathrm{i}\tan\delta)\,, \tag{1}$$

is shown as mastercurves in Fig. 1, which have been determined from dynamic mechanical analyses (DMA). The real part of the complex mod-

Table 3
Properties of the two KRAIBON® compounds SAA9579/52 (E1) and HAA9275/45 (E2) studied in this work according to data sheets supplied by the manufacturer [41,42].

	SAA9579/52 (E1)	HAA9275/45 (E2)
Base polymer	EPDM	EPDM
Mass density	1180 $\mathrm{kg\,m^{-3}}$	1250 $\mathrm{kg\,m^{-3}}$
Hardness	88 Shore A	98 Shore A

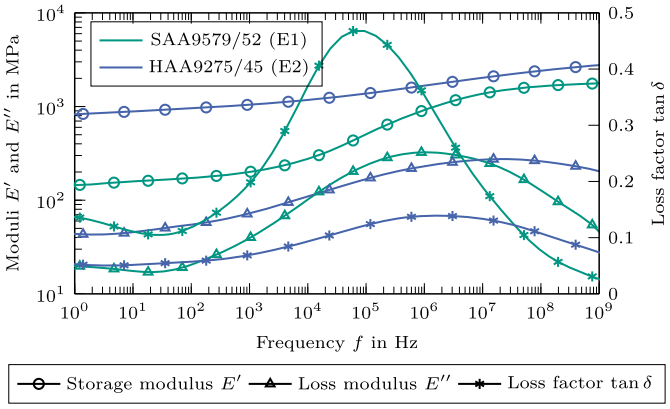

Fig. 1. Mastercurves of the two elastomer compounds studied in this work. The curves are determined by DMA experiments and time-temperature superposition for rheological simple materials. The curves show the viscoelastic behavior of both compounds at a temperature of $T = 20\,°\mathrm{C}$.

ulus, E', quantifies the purely elastic part of the viscoelastic behavior and is referred to as the storage modulus. The imaginary part E'' describes the purely viscous and thus dissipative contribution, accordingly called loss modulus. A measure of the present material damping is given by the loss factor

$$\tan\delta = \frac{E''}{E'} \tag{2}$$

which is dimensionless and indicates the fraction of dissipated energy and elastically stored energy under periodic steady-state loading. The mastercurves shown in Fig. 1 highlight the differences in viscoelastic behavior of the two elastomers. When comparing the storage moduli, a significantly higher stiffness of elastomer E2 is observed. Although both materials show a strong frequency dependence, the same is more pronounced for elastomer E1. Additionally, E1 features overall higher material damping as indicated by the loss factor curve.

The HyCEMLs in this work are studied in four different configurations, which are listed in Table 4. Two configurations feature aluminum plies on the outside, whereas the other two have stacks of CFRP plies at the top and bottom. Furthermore, each lamination scheme is investigated with the two aforementioned elastomer damping plies, yielding four configurations in total. Notably, all laminates feature the same volume content of elastomer damping plies and have the same overall thickness.

The hybrid laminates introduced above are manufactured in a single hot-mold process, where the stack of neat constituents is consolidated at a pressure of 40 bar for 300 s while maintaining a temperature of 150 °C. It should be noted that no additional adhesive or surface treatment is used, as the elastomers vulcanize directly onto the other two substrates, which are degreased with acetone prior to stacking.

2.2. Experimental methods

In order to induce damage into the laminates, low-velocity impact tests are carried out. These experiments are conducted as instrumented dropweight tower tests on a Coesfeld Magnus 1300 machine

Table 4
HyCEML configurations with two different elastomers. All laminates have the same overall thickness of 2.5 mm. Ply thickness is specified by the indices. Superscripts state the material orientation relative to the x-axis along the plates' longer edge.

Laminate	Abbreviation
$\left[\mathrm{A}_{0.3}/\mathrm{E1}_{0.5}/\left(\mathrm{C}^{0°}_{0.15}/\mathrm{C}^{90°}_{0.15}\right)_3/\mathrm{E1}_{0.5}/\mathrm{A}_{0.3}\right]$	AE1C
$\left[\mathrm{A}_{0.3}/\mathrm{E2}_{0.5}/\left(\mathrm{C}^{0°}_{0.15}/\mathrm{C}^{90°}_{0.15}\right)_3/\mathrm{E2}_{0.5}/\mathrm{A}_{0.3}\right]$	AE2C
$\left[\left(\mathrm{C}^{0°}_{0.15}/\mathrm{C}^{90°}_{0.15}\right)_s/\mathrm{E1}_{0.5}/\mathrm{A}_{0.3}/\mathrm{E1}_{0.5}/\left(\mathrm{C}^{0°}_{0.15}/\mathrm{C}^{90°}_{0.15}\right)_s\right]$	CE1A
$\left[\left(\mathrm{C}^{0°}_{0.15}/\mathrm{C}^{90°}_{0.15}\right)_s/\mathrm{E2}_{0.5}/\mathrm{A}_{0.3}/\mathrm{E2}_{0.5}/\left(\mathrm{C}^{0°}_{0.15}/\mathrm{C}^{90°}_{0.15}\right)_s\right]$	CE2A

with boundary conditions and specimen preparation adhering to ASTM D7136. Plate specimens with a length of 150 mm and a width of 100 mm are cut by using a iCUTwater SMART waterjet cutting machine by imes-icore GmbH. The specimens are then placed on a flat support fixture with a rectangular cutout of 100 mm × 75 mm and clamped down by four clamps with rubber tips in order to hold down the specimen during the impact event. The semi-spherical impactor used in the experiments has a diameter of 20 mm and a mass of 5.25 kg. For all laminates, the impact energy U_{impact} is varied by changing the drop height so that levels of 5 J, 10 J and 20 J are achieved. All impact events are recorded by a high speed camera in order to assess the impact event for possible rebounds or other potential errors. The support fixture, holding clamps, impactor and a specimen during impact can be seen in Fig. 2. Five specimens are tested for each laminate and impact energy, totaling in 60 experiments.

The damage, caused by the impact events, is assessed by cutting small samples from the damaged plates with an Accutom wet cut-off machine from Struers at very low speeds to prevent any further damage progression. The samples are embedded in epoxy resin for subsequent light microscopy analyses.

2.3. Numerical methods

Following the damage assessment of impacted specimens outlined in Section 2.2, numerical FEM models are deployed in order to investigate how the observed damage modes influence the CLD mechanism in HyCEML. The modeling approach for these damage modes is introduced in the following paragraphs.

2.3.1. Modeling of impact damage

Intra-ply damage The effect of intra-ply damage within the CFRP plies is modeled as a stiffness degradation based on the progressive damage model proposed by Lapcyk and Hurtado [43]. For states of plane stress, as imposed by a continuum shell formulation, the constitutive relation is given by

$$\begin{bmatrix}\sigma_{11}\\ \sigma_{22}\\ \sigma_{12}\end{bmatrix} = \frac{1}{d}\begin{bmatrix}\left(1-d_\mathrm{f}\right)E_1 & \left(1-d_\mathrm{f}\right)\left(1-d_\mathrm{m}\right)\nu_{21}E_1 & 0\\ \left(1-d_\mathrm{f}\right)\left(1-d_\mathrm{m}\right)\nu_{12}E_2 & \left(1-d_\mathrm{m}\right)E_2 & 0\\ 0 & 0 & \left(1-d_\mathrm{s}\right)dG_{12}\end{bmatrix}\cdot\begin{bmatrix}\varepsilon_{11}\\ \varepsilon_{22}\\ \gamma_{12}\end{bmatrix} \tag{3}$$

depending on three damage parameters. Parameter d_f models the degree of fiber damage, whereas d_m represents matrix damage. In this context, no distinction between tension and compression is made for the fiber and matrix damage parameters d_f and d_m as this would be obsolete in the subsequent modal analyses. Interface shear damage is accounted for by the damage parameter

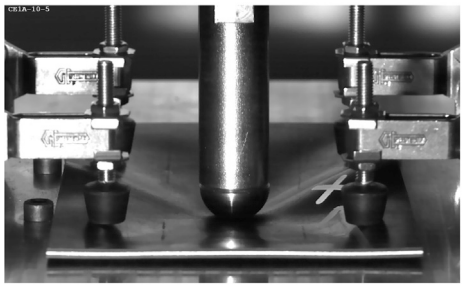

Fig. 2. Low-velocity impact test on a hybrid laminate according to ASTM D7136. The plate's visible edge has a length of $b = 100$ mm.

$$d_s = 1 - \left(1 - d_f\right)^2 \left(1 - d_m\right)^2 \tag{4}$$

A combined damage parameter d is introduced as shown by Equation (5).

$$d = 1 - \left(1 - d_f\right) \left(1 - d_m\right) \nu_{12} \nu_{21}. \tag{5}$$

The above constitutive relation is implemented depending on the prescribed damage parameters d_f and d_m as a user-defined material subroutine UMAT in Abaqus/Standard. This allows for the direct specification of arbitrary states of damage via the introduced damage parameters without the need for damage initiation and evolution, respectively. In order to account for the state of degradation outlined above, plane stress is enforced by the use of continuum shell elements SC8R for all CFRP plies.

Delaminations The occurrence of delaminations after impact in arbitrary plies is modeled based on an unconstrained approach as first proposed by Wang et al. [23]. This modeling approach is chosen as it represents the lower bound for the natural frequency of the delaminated structure [32] and is thus assumed to also represent the lowest load transmission into the damping layers, making it the worst case for the CLD mechanism. Opening of delaminations during vibration, which has been reported to occur in experiments by Shen and Grady [25] and subsequent papers, is allowed by this approach. Penetration of the two domains, however, is not prevented. Furthermore, this approach, as opposed to modeling the delamination with cohesive elements, does not introduce an additional thickness into the laminate, facilitating comparisons with undamaged models without any interface modeling. The laminated plate is divided into separate domains at interfaces in which a delamination is to be modeled. The delaminated area of arbitrary shape and size is thus described by one surface each on both domains. The surfaces making up the remainder of the interface, which is not delaminated, are permanently bonded using a kinematic tie constraint, preventing any relative motion. This tie constraint is resolved on the two surfaces forming the delamination.

Permanent deformation In this work, the permanent deformation of impacted laminates is modeled by a stress-free mesh deformation approach. First, a finite element model of the undeformed laminate is created. Subsequently, all nodes are translated in transverse direction based on an analytical function $w = f(x, y)$ describing the predeformed structure. As this corresponds to a simple shear deformation, this mesh transformation is isochoric, thus not changing volume or mass of the model. The function used throughout this work is a modified Gaussian function and is given by

$$w(x, y) = -w_{\max} e^{-\left((x/a-0.5)^2+(y/b-0.5)^2\right)s^{-1}}, \tag{6}$$

where $w_{\max}$ is the maximum permanent translation in z-direction. Parameters a and b correspond to the rectangular plate's in-plane dimensions in x- and y-direction, respectively. The origin of the coordinate system lies in the corner of the plate. Furthermore, the parameter s controls the localization of the permanent deformation towards the center of the plate, respectively the location of impact. The influence of this parameter s is shown in Fig. 3, where higher values of s signify a less localized deformation.

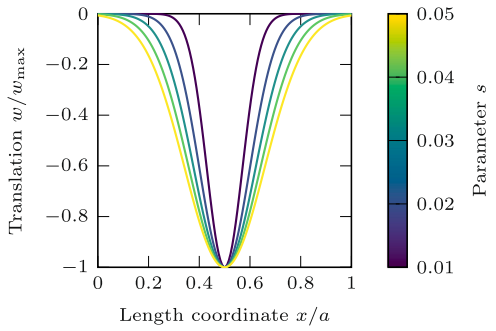

Fig. 3. Normalized display of $w(x, y)$ in Equation (6) for $y = b/2$. The figure shows the deflection distribution for multiple values of s. Smaller values of s lead to a more localized deformation.

2.3.2. Analyzing the effect of damage on CLD

The modeling approaches introduced above are utilized to numerically assess, how different states of damage influence the damping behavior of HyCEML. The three individual modes of damage introduced above are investigated individually and include, but are not limited to, those seen in the accompanying experiments. The corresponding numerical parametric studies are introduced in the following paragraphs and illustrated in Fig. 4. In each case, an impacted plate of dimensions $a = 150$ mm and $b = 100$ mm is considered. All four configurations of HyCEML listed in Table 4 are investigated. Fig. 5 shows the naming convention for plies and interfaces used for the two groups of laminates, namely CE1A and CE2A (left) as well as AE1C and AE2C (right).

Abaqus/Standard is used to model the laminates. The laminates are modeled as solid 3D deformable bodies. Each material layer is discretized by three elements over its thickness. CFRP layers are modeled using linear continuum shell elements SC8R with reduced integration and the linear elastic parameters listed in Table 1. Quadratic continuum elements of type C3D20R with reduced integration are chosen for the aluminum plies, which are also assumed linear elastic based on the constants in Table 2. Reduced integration hybrid elements C3D20RH are used to model the elastomer layers. By direct specification of the frequency-dependent complex modulus presented in Fig. 1 the elastomers' linear viscoelastic behavior is modeled in the frequency domain.

Complex modal analysis is conducted with a property evaluation frequency of $f_{\text{eval}} = 1500$ Hz, which is chosen as it approximately represents the middle of the interval, in which the natural frequencies are found. The resulting natural frequencies

$$f_n = \frac{|\Im\left(\lambda_n^*\right)|}{2\pi} \tag{7}$$

and effective modal damping ratios

$$\xi_n = -2\frac{\Re\left(\lambda_n^*\right)}{|\Im\left(\lambda_n^*\right)|} \tag{8}$$

are calculated from the complex eigenvalue λ_n^* of the n^{th} vibration mode of the complex eigenvalue problem

$$\left(\lambda_n^{*2}\mathbf{M} + \mathbf{K}^*\right)\mathbf{\Phi}_n^* = \mathbf{0} \tag{9}$$

with the complex valued stiffness matrix $\mathbf{K}^*$, mass matrix $\mathbf{M}$ and the n^{th} complex eigenvector $\mathbf{\Phi}_n^*$ of the FEM model. A comparison of the natural frequencies and modal damping ratios of the first ten vibration modes is then made between undamaged and damaged laminates.

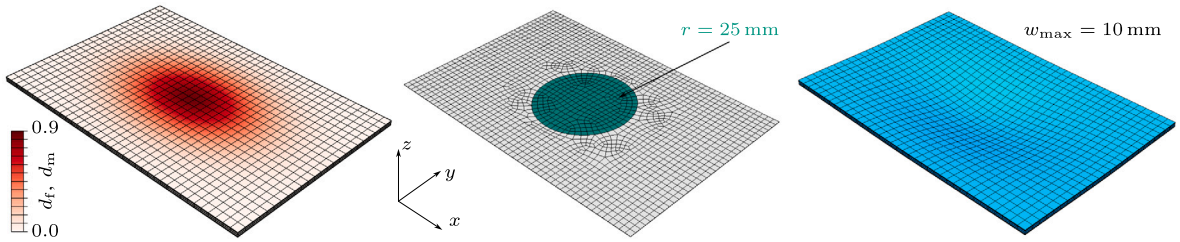

Fig. 4. Finite element models of three different types of damage: intra-ply damage (left), delamination (center) and permanent deformation (right). All types have their maximum extent in the plate's center.

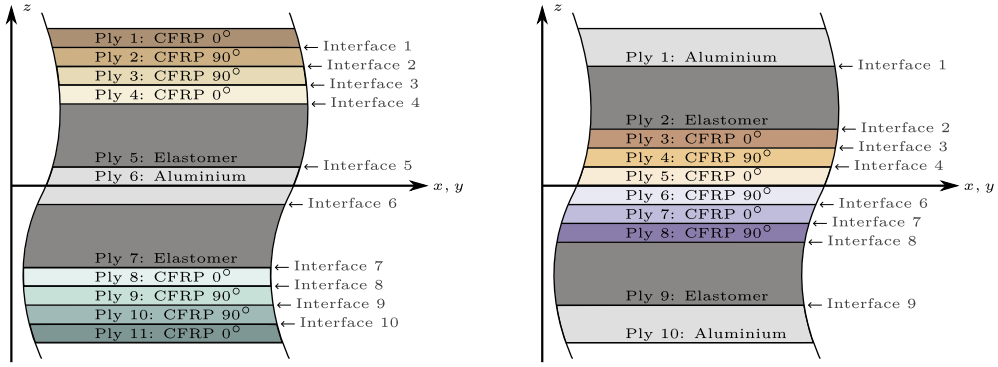

Fig. 5. Schematic layup of both types of HyCEML investigated in this study. Plies and interfaces are numbered accordingly. Both types have the same overall thickness and the same volume fraction of elastomer material. Laminates CE1A and CE2A follow the layup on the left, whereas laminate AE1C and AE2C correspond to the layup on the right. Dimensions are not to scale.

Intra-ply damage The influence of a decrease in the load-bearing capabilities of the CFRP plies on the CLD mechanism in HyCEML is analyzed in the following. For this purpose, intra-ply damage is assumed to occur in each CFRP ply separately, thus allowing the identification of critical plies within the laminates. The maximum value of the fiber damage parameter in Equation (3) is assumed to be $d_{f,max} = 0.9$. Additionally, the same value is assumed for the maximum matrix damage parameter with $d_{m,max} = 0.9$ yielding a maximum shear damage parameter of $d_{s,max} \approx 1$. This state is visualized in Fig. 4. For the critical plies determined this way, the two damage parameters $d_{f,max}$ and $d_{m,max}$ are further varied in the range from 0 to 1 in order to investigate how both, fiber and matrix damage, influence the CLD mechanism.

Delaminations As, within the scope of this work, delaminations can theoretically occur in all interfaces of the laminates, a first study aims at the identification of critical interfaces, in which possible delaminations have the highest influence on the vibration and damping behavior. Therefore, a single hypothetical circular delamination with radius $r = 25$ mm located on the plate's center point, thus the point of impact, is assumed to occur in each interface individually, including those interfaces, where delaminations are observed in the accompanying experiments. For one interface, this delamination is visualized in Fig. 4. Subsequently, the influence of delamination size is investigated for select interfaces.

Permanent deformation The influence of permanently deformed HyCEMLs is studied by means of multiple deformed plates according to Equation (6). The maximum deformation specified by the parameter w_{max} is varied in the range of 0 mm to 10 mm, which encompasses the deformation observed in the impact experiments, with an increment of 1 mm with the distribution parameter $s = 0.05$. For each laminate, identical meshes are used prior to the predeformation of the mesh. A permanently deformed mesh of $w_{max} = 10$ mm is shown in Fig. 4.

3. Results and discussion

3.1. Experimental

The results of the dropweight experiments according to ASTM D7136 are summarized in Fig. 6 for the four laminates under investigation. The first row of graphs shows the recorded impact force F over time t of the impact event. The onset of damage, indicated by the occurrence of oscillations in the curve, can be identified. No damage is observed for impact energies of 5 J, whereas all laminates except CE1A show signs of damage from 10 J upwards. In all cases, damage occurs at impact forces of approximately 3000 N, which is assumed to be the onset of either delaminations or cracking of the CFRP plies. The highest forces are observed in laminate CE2A. The force-displacement curves give an indication of the remaining deformation after the impact event, hereafter referred to as permanent deformation. Generally, laminates AE1C and AE2C exhibit higher permanent deformations than those laminates where the CFRP plies are located on the outside, which can be attributed to the higher amount of plastically deforming aluminum plies. The contributions of the individual modes of damage to the overall absorbed energy under similar impact conditions are studied in [10] using the example of laminate AE1C. It should be noted, that the experiments exhibit very low scatter with regard to maximum force, maximum displacement as well as the calculated impact energy over time, attesting to the soundness of the experimental procedure.

Fig. 7 shows post-impact microsections of laminates impacted with 10 J. Laminate CE1A only shows a slight permanent deformation with no other types of damage visible. The laminate with the stiffer elastomer, CE2A, shows a delamination as well as a crack in the bottom CFRP ply. Impacted laminates AE1C and AE2C feature significant higher levels of permanent deformation as well as intra-ply damage in all CFRP plies. There are also visible delaminations of the lower CFRP plies. The types of damage observed in these micrographs are consistent with the force and displacement curves presented in Fig. 6 as well as

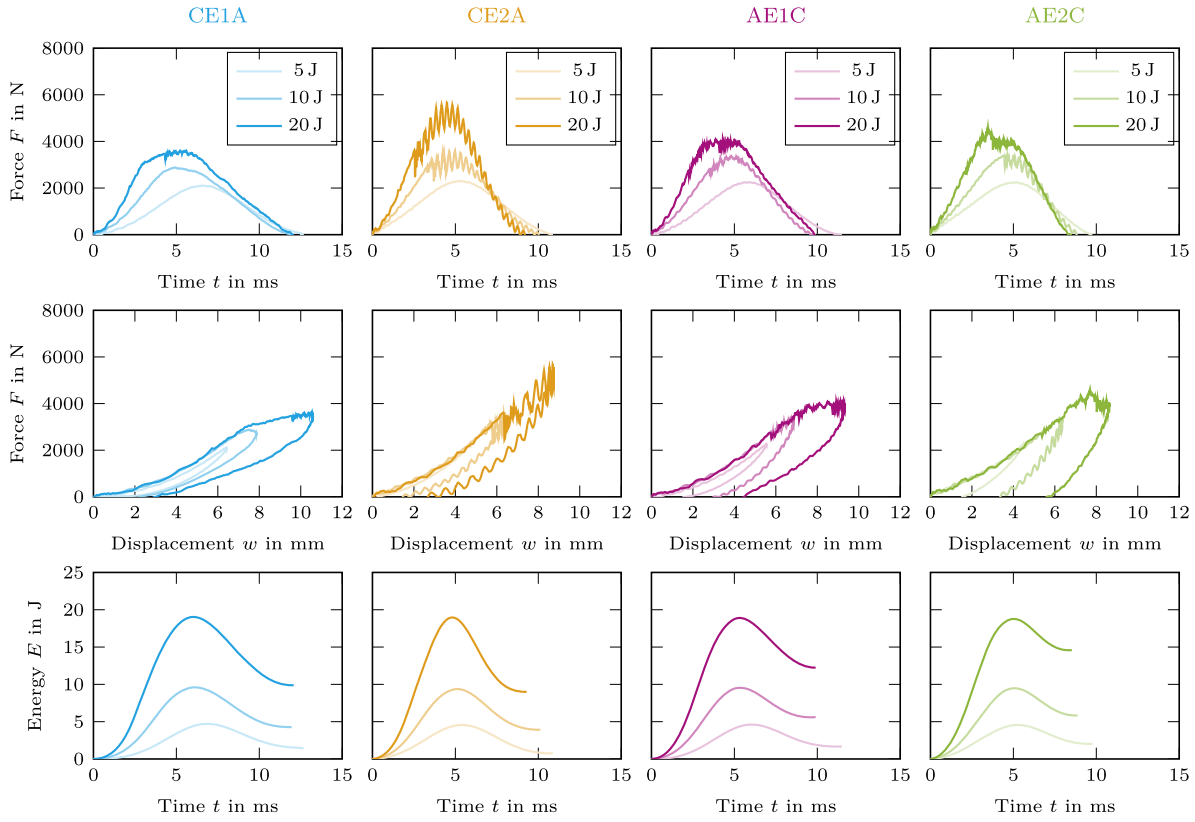

Fig. 6. Results of low-velocity dropweight experiments for three different impact energies and four different HyCEML laminates. Different laminates are indicated by individual colors.

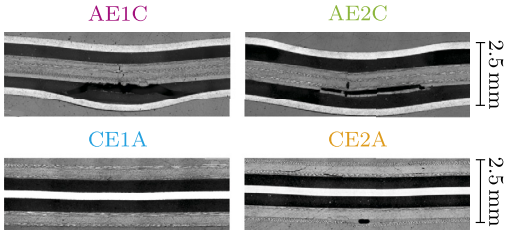

Fig. 7. Microsections of four damaged laminates impacted with an impact energy of 10 J. Visible types of damage include intra-ply failure in CFRP plies, delaminations and permanent deformation. Layups according to Fig. 5. All laminates have identical initial thickness.

those typically found in conventional FMLs [44]. Given the large deflections of the laminates during impact, see Figure 6, it can be assumed, that the compliant elastomer plies undergo severe deformation, which can cause cyclic softening often observed in filled elastomers and commonly referred to as Mullins effect [45,46]. As this effect is the subject of an ongoing study by the authors, it will not be considered further within this paper. Overall, the observed types of damage are consistent with those presented in literature, for example in [15,16] for FMELs containing layers of steel instead of aluminum.

3.2. Numerical

3.2.1. Undamaged laminates

The results of modal analysis on undamaged laminates are shown in Fig. 8 for the four different configurations of HyCEML in terms of natural frequencies f_n and their corresponding modal damping ratios ξ_n. Damaged laminates will be compared to those results in the subsequent sections.

For each laminate, the first ten vibration modes are considered, which correspond to the mode shapes listed in Table 5. It can be noted that the occurrence and order of specific modes varies between different laminates.

The results in Fig. 8 show that the four laminates have similar stiffness as their natural frequencies lie in proximity. When considering the higher modes, laminates CE2A and AE2C appear to be stiffer than laminates CE1A and AE1C, suggesting that the stiffness of the elastomer has a higher influence on the natural frequency than the general layup of the laminate. A comparison of the modal damping ratios shows significantly higher damping of laminates CE1A and AE1C compared to the other two laminates containing the elastomer E2. These results are in accordance with expectations, as from Fig. 1 a higher loss factor $\tan\delta$ is observed in the given frequency range. Again, the choice of the elastomer damping material has a stronger influence than the choice of the general laminate layup.

3.2.2. Influence of intra-ply damage

Fig. 9 shows the relative changes in natural frequencies and modal damping ratios compared to an undamaged laminate of the same configuration for individual intra-ply damages in different CFRP plies according to Fig. 5. The ten vibration modes listed in Table 5 are considered.

In all cases, the presence of intra-ply damage leads to lower natural frequencies due to a reduced overall bending stiffness, although a strong dependence on the present mode as well as occasional mode shifts are observed. While the reduction in natural frequencies can reach up to approximately 8% for laminates CE1A and CE2A, the decrease lies well below 1% for laminates AE1C and AE2C. As laminates CE1A and CE2A are balanced laminates, see Fig. 5, opposite plies such as Ply 1 and Ply 11 or Ply 3 and Ply 9 yield identical results. Laminates AE1C and AE2C on the other hand show asymmetrical results in this regard, being unbalanced laminates. When considering the relative changes in

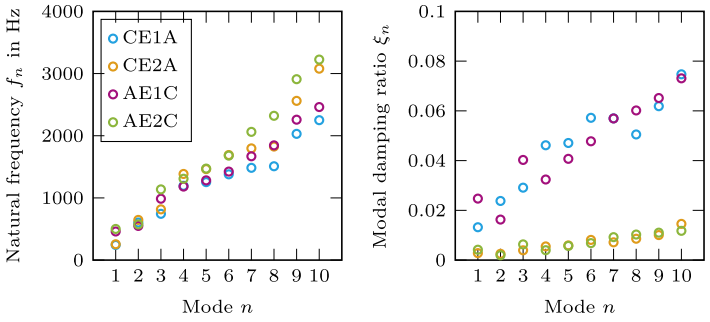

Fig. 8. Natural frequencies (left) and modal damping ratios (right) of undamaged HyCEML plates for their first ten vibration modes listed in Table 5.

Table 5
First ten mode shapes of undamaged laminates corresponding to the natural frequencies and modal damping ratios in Fig. 8. The x- and y-axes run along the long and short edge, respectively. Colors indicate the normalized translation in transverse direction. The occurrence of specific modes is dependent on the laminate in some cases.

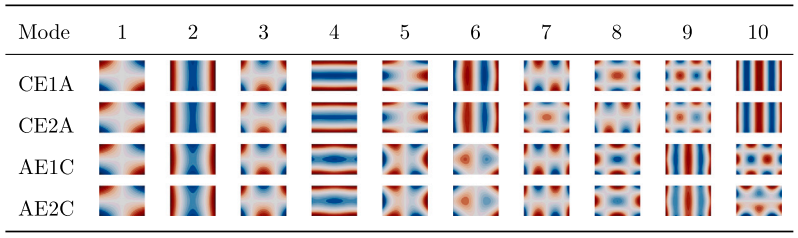

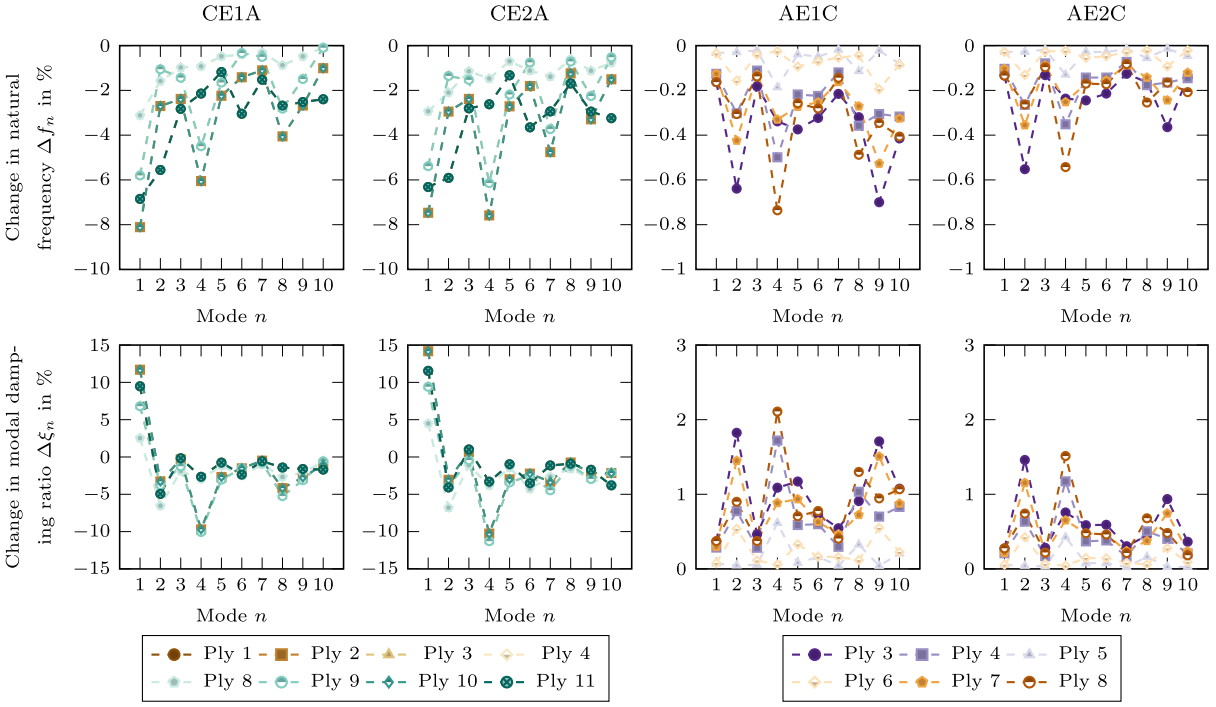

Fig. 9. Relative change in natural frequencies and modal damping ratios of the vibration modes listed in Table 5 compared to an undamaged plate (Fig. 8). Results are displayed for four different HyCEML configurations and different individual CFRP plies affected by the intra-ply damage described in Section 2.3.2 and Fig. 4.

modal damping ratios, laminates CE1A and CE2A show both, positive and negative changes. Mode 1 for example, shows a higher damping ratio for damage in all plies, whereas Mode 4 exhibits a minimum in modal damping for damage in Ply 2 and Ply 10. Modal damping ratios of laminates AE1C and AE2C are generally influenced to a smaller extent by intra-ply damage, however, the change is invariably positive. As with the other two laminates, Mode 4, which shape is identical for all laminates, is influenced the strongest.

In order to identify critical plies, in which intra-ply damage has the strongest influence on the CLD mechanism, the median relative change in natural frequency and modal damping ratio of the first ten vibration modes is considered for damage in each ply. These results are shown as box plots in Fig. 10 for all four laminates.

When observing the median change in natural frequencies, the predominant role of intra-ply damage in the outermost CFRP plies is evident in the reduction of natural frequencies. Generally, the median

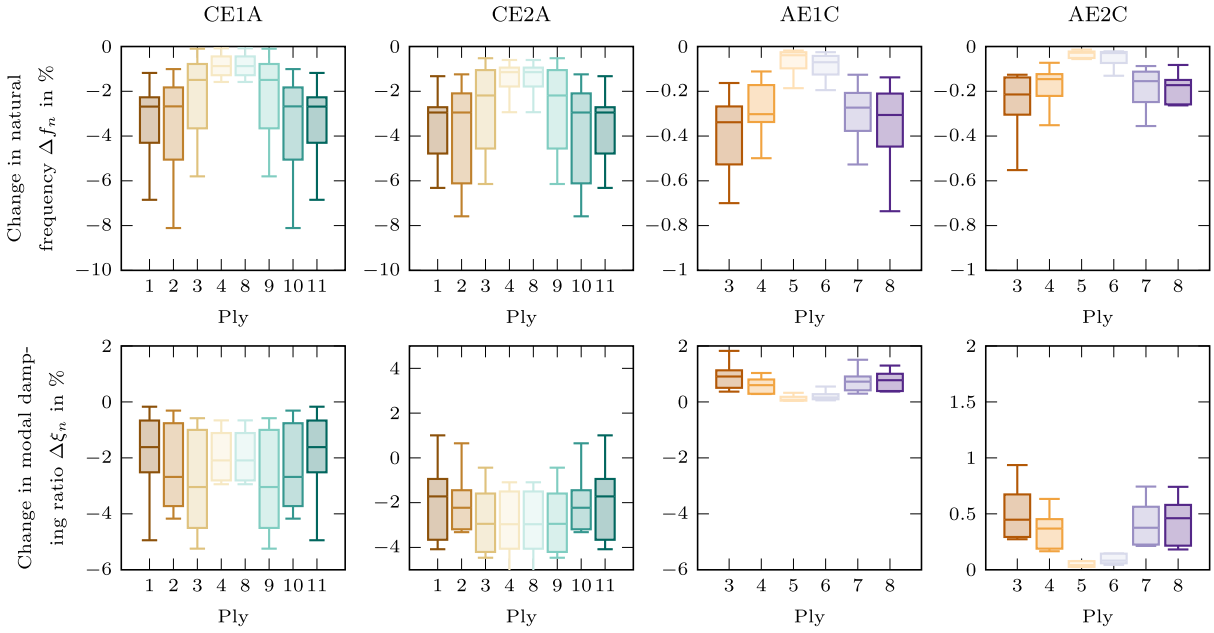

Fig. 10. Box plots showing the change of natural frequency and modal damping ratio of the first ten vibration modes caused by intra-ply damage according to Fig. 4 in the individual CFRP plies corresponding to Fig. 5. Plots show the median values, the lower and upper quartiles as boxes and the minimum and maximum change values as whiskers.

change in natural frequencies is less pronounced by an order of magnitude for laminates AE1C and AE2C compared to the other two laminates, in which the CFRP plies are located further out (see Fig. 5). Notably, laminates AE1C and AE2C exhibit median changes in natural frequencies, which are unsymmetrical with regard to the stacking sequence. Upon consideration of median changes in modal damping ratios, it is noticeable that laminates CE1A and CE2A exhibit lower modal damping ratios as a result of intra-ply damage, whereas in laminates AE1C and AE2C intra-ply damage leads to an increase in modal damping. Here, especially intra-ply damage in Ply 3 and Ply 8 result in a comparably high median change in modal damping, as these are the plies adjacent to the elastomer damping layers. A similar observation can be made for laminate CE2A, where damage in Ply 4 and Ply 8 influence the modal damping ratio the strongest. In laminate CE1A, however, the two 90°plies lead to the highest median change as a result of intra-ply damage. Another aspect which can be taken from Fig. 10 concerns the choice of elastomer used in HyCEML. The application of the softer elastomer E1, compare Fig. 1, leads to a higher damage tolerance in laminate CE1A compared to laminate CE2A, both in terms of stiffness reduction and modal damping ratios. This observation is inverted when comparing laminates AE1C and AE2C, where the stiffer elastomer E2 yields the higher tolerance to the given states of intra-ply damage.

Fig. 11 shows the influence of damage parameters $d_{\mathrm{f,max}}$ and $d_{\mathrm{m,max}}$ for an intra-ply damage in Ply 4 in laminate CE1A, which is adjacent to the elastomer damping layer and, according to Fig. 10, has the highest median influence on modal damping. Depicted are the natural frequencies and modal damping ratios of the first four vibration modes according to Table 5 relative to the undamaged state. The contour lines represent states of equal damage regarding a change in natural frequency or modal damping ratio, respectively. While for Mode 1, fiber as well as matrix damage seem to have an equal influence on both, natural frequency and modal damping ratio, Mode 2 is dominated by fiber damage alone. Modes 3 and 4 show a significantly lower dependence on intra-ply damage, see Fig. 9. Similar results are obtained for other laminates, but are omitted for brevity.

Generally, the findings presented regarding the influence of intra-ply damage on CLD feature a strong dependence on the vibration mode at hand. This has also been reported by Gröhlich et al. [47] for thermal impact on CLD beams. Nevertheless, lamination scheme and choice of elastomeric damping material do have an influence on the damage tolerance of the CLD mechanism in HyCEMLs. Naturally, laminates of type AEC are more tolerant to intra-ply damage in CFRP plies, as these are positioned closer to the neutral plane of the laminate, thus mitigating the effect of present damages. Fiber damage also has a higher impact on the vibrational behavior than matrix damage, an effect also reported in [38].

3.2.3. *Influence of delaminations*

The relative changes in natural frequencies and modal damping ratios compared to the undamaged plate of the same laminate type are shown in Fig. 12 for individual delaminations of radius $r = 25$ mm in different interfaces according to Fig. 5. It should be noted, that only the modes listed in Table 5 are compared hereafter, but due to the unconstrained modeling approach, a number of additional opening modes of the delaminated areas are observed. Similar observations are reported in [32,34,35] for this type of modeling approach. These additional modes are also present in forced vibration as shown in Appendix A. Furthermore, more mode shifts than seen for intra-ply damage are present, meaning that the mode shapes shown in Table 5 occur in a different order, which is also reported for thermal impact on CLD beams [47]. Laminates CE1A and CE2A show symmetric results regarding their neutral plane following their symmetric layup, whereas the other two laminates do not. Generally, the presence of a delamination leads to a decrease in natural frequencies in most cases. There are, however, exceptions, such as a delaminated Interface 3 and Interface 8 in laminates CE1A and CE2A, for some modes. In these cases, the vibration mode of the damaged laminate is a superposition of the global mode, as shown in Table 5, and an opening mode, thus local mode, of the delaminated sublaminate. These observations are in agreement with those of Chen [35] made for delaminated composite beams. For all laminates and both, natural frequencies and modal damping ratios, a strong mode dependency exists with changes in modal damping of up to 40%. Laminates CE1A and CE2A show the highest changes in natural frequency and modal damping ratios for delaminations in interfaces between CFRP layers with 0°and 90°orientation for some modes. These are also the delaminations observed experimentally and visible in Fig. 6. Laminate CE2A

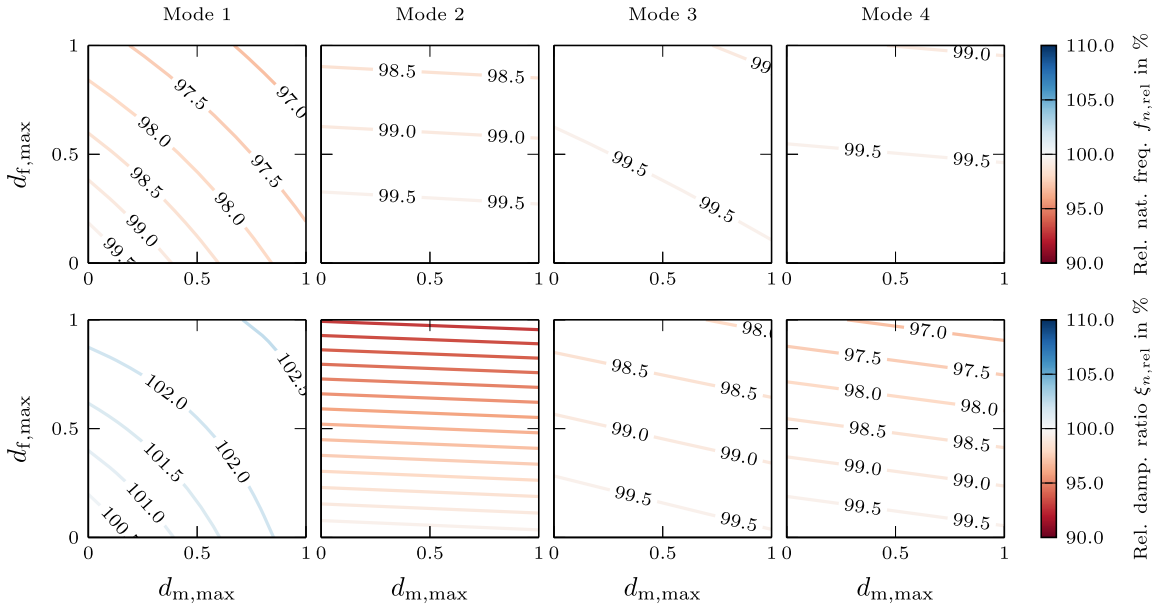

Fig. 11. Relative natural frequencies (top) and relative modal damping ratios (bottom) of laminate CE1A for different values of maximum fiber damage $d_{f,max}$ and maximum matrix damage $d_{m,max}$ in Ply 4 (see Fig. 5) for the first four vibration modes. Contour lines represent damage of equal extent regarding change in natural frequency or modal damping ratio. Note: Contour line labels are omitted for Mode 2 for sake of readability.

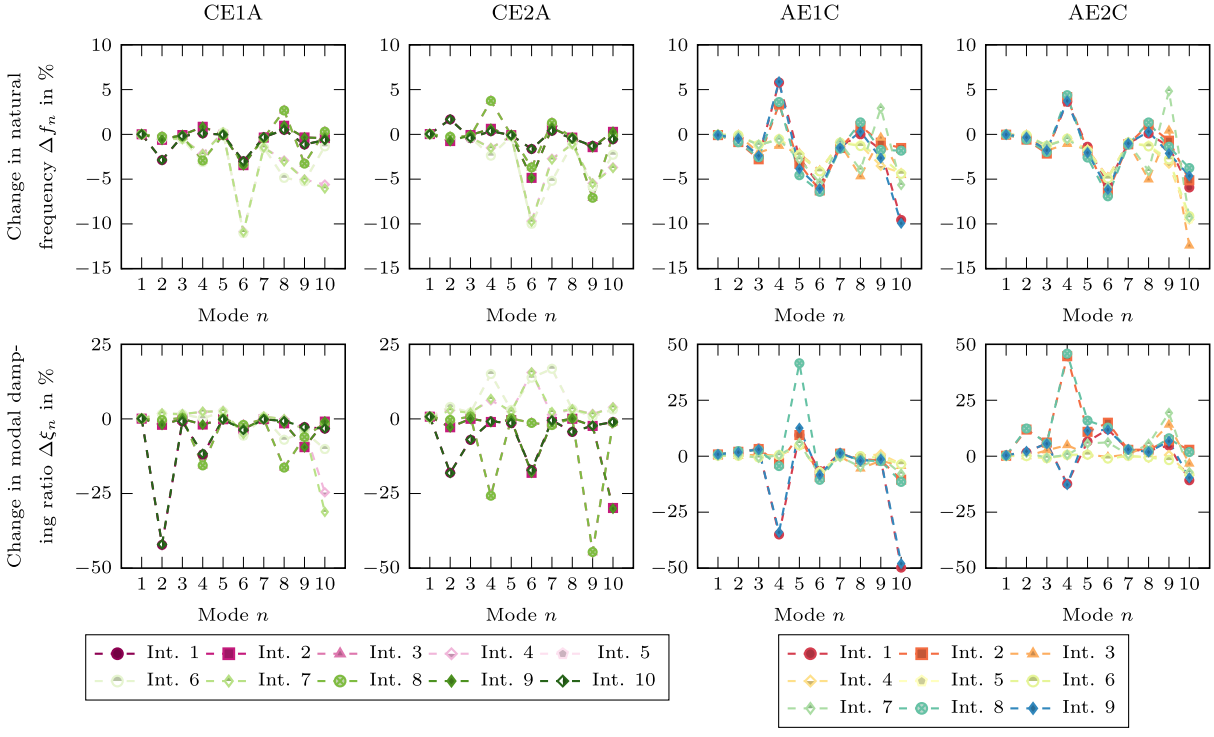

Fig. 12. Relative change in natural frequencies and modal damping ratios of the vibration modes listed in Table 5 compared to an undamaged plate (Fig. 8). Results are displayed for delaminations in different interfaces.

also shows a high loss in stiffness when Interface 5 and Interface 7, which connect the elastomer layer, delaminate, highlighting the structural load-bearing role of the stiffer elastomer E2 compared to the softer elastomer E1 in laminate CE1A. The greatest changes in natural frequency and modal damping ratio in laminates AE1C and AE2C are also observed when interfaces connecting the elastomer layers are damaged. Generally, the choice of elastomer has a smaller influence on the vibrational behavior of delaminated laminates of type AEC than on laminates CEA.

Fig. 13 shows the median change in natural frequencies and modal damping ratios over the first ten vibration modes caused by delaminations in the individual interfaces. For all laminates, the median change in natural frequency is negative, with laminates AE1C and AE2C being more sensitive to delaminations in the median of ten vibration modes than the other two laminates. While delaminations in AE1C and AE2C show a similar median influence on the natural frequencies, the innermost interfaces in CE1A and CE2A, namely those adjacent to the elastomer layers, have a significantly higher influence than those be-

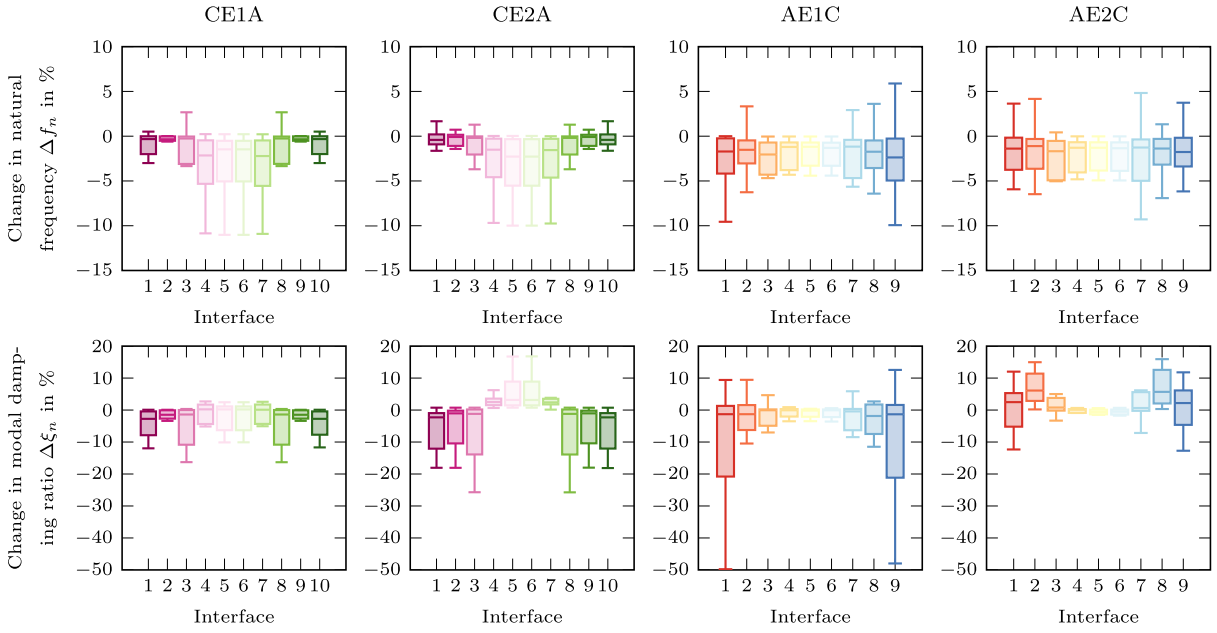

Fig. 13. Box plots showing the change of natural frequency and modal damping ratio of the first ten vibration modes caused by delaminations in individual interfaces, according to Fig. 5. Plots show the median values, the lower and upper quartiles as boxes and the minimum and maximum change values as whiskers.

tween CFRP plies. Laminate AE1C hardly shows any median change in modal damping ratios, which can be attributed to the fact that, as seen in Fig. 12, change values oscillate around zero. Very high median changes in modal damping ratios are present for delaminations adjacent to the stiff elastomer layers in laminate AE2C.

Fig. 14 shows how the size of the delaminated area influences the modal parameters exemplary for the second vibration mode according to Table 5. A single circular delamination of varying radius in an interface between the CFRP and elastomer plies, i.e. in Interface 4 for laminate type CEA and in Interface 2 for type AEC, is considered. All four laminates hardly show any change in natural frequency for delaminations smaller than 10% of the overall interface area. From this point onward, however, a linear decrease in natural frequency is observed for laminates AE1C and AE2C. Laminates CE1A and CE2A show a slower decrease of the second natural frequency. Laminates containing the stiffer elastomer E2 exhibit a slightly lower vulnerability towards increasing delamination size in the interfaces considered here. The modal damping ratios of the second vibration mode generally show an increase for larger delaminations. Notably, this effect is the most pronounced for laminate AE2C. Laminate AE1C shows a decrease for delaminations exceeding 20%. Although superimposed opening modes of delaminated areas also occur in laminate AE2C, this decrease in modal damping ratios is unique among the configurations studied here. In fact, this is explained by the way the elastomer Ply 2 is deformed in the superimposed opening mode. This opening mode is driven by the much stiffer aluminum Ply 1, leading to high shear deformations of the bonded elastomer layer, creating a free-layer damping (FLD) effect. This is, however, far less effective for the very compliant elastomer E1 leading to lower modal strain energies in the material. Consequently, only one of the two elastomer layers takes part in the dissipation of vibration energy as the CLD mechanism is far more effective, especially for softer materials. For stiffer materials, however, FLD becomes dominant, resulting in the strong increase in modal damping seen for laminate AE2C. Laminates CE1A and CE2A, in this example of the second vibration mode, do not show any opening modes of delaminated areas. These correlations have been outlines for the second vibration mode only and might be different for other modes, highlighting the strong mode dependency of CLD in damaged laminates.

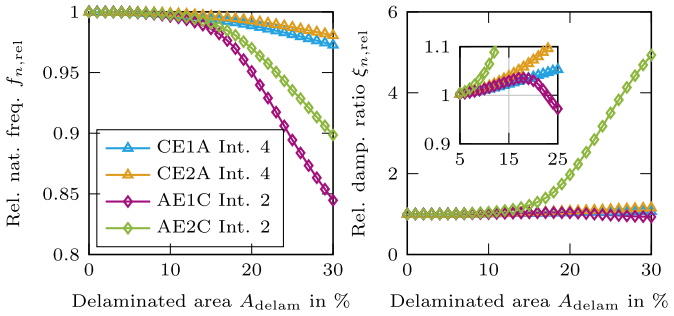

Fig. 14. Influence of delamination size on the second vibration mode according to Table 5 for delaminations in critical interfaces.

3.2.4. *Influence of permanent deformation*

Changes of natural frequencies and modal damping ratios of predeformed HyCEML plates are shown in Fig. 15. Results are shown for the four HyCEML configurations and different levels of permanent deformation, which are defined by the parameter w_{max} in Equation (6).

All levels of permanent deformation in each laminate lead to an increase in the natural frequencies of all vibration modes considered. Generally, higher levels of permanent deformation act as beads, yielding a higher plate stiffness. The extent to which individual natural frequencies are shifted, however, shows a strong mode dependency. For laminates CE1A and CE2A, the first vibration mode shows the largest shifts, especially for higher values of w_{max}. Mode 8 in case of laminate CE1A and Mode 7 for laminate CE2A also show high shifts compared to other modes. In fact, this is the same vibration mode in both laminates according to Table 5, indicating that both laminates are stiffened in a very similar manner by the permanent deformation. Laminates AE1C and AE2C exhibit the largest shift in natural frequencies for Mode 2 and Mode 9, which happen to be the first and third one-dimensional longitudinal bending modes according to Table 5. The second one-dimensional bending mode, Mode 6, also shows a comparably high shift in natural frequencies, especially for laminate AE1C. The relative change in modal damping ratios, in contrast, does not show trends as uniform as the change in natural frequencies. While most states of permanent deformation lead to less modal damping for the majority of modes, exceptions can be observed. In case of laminates CE1A and CE2A, for ex-

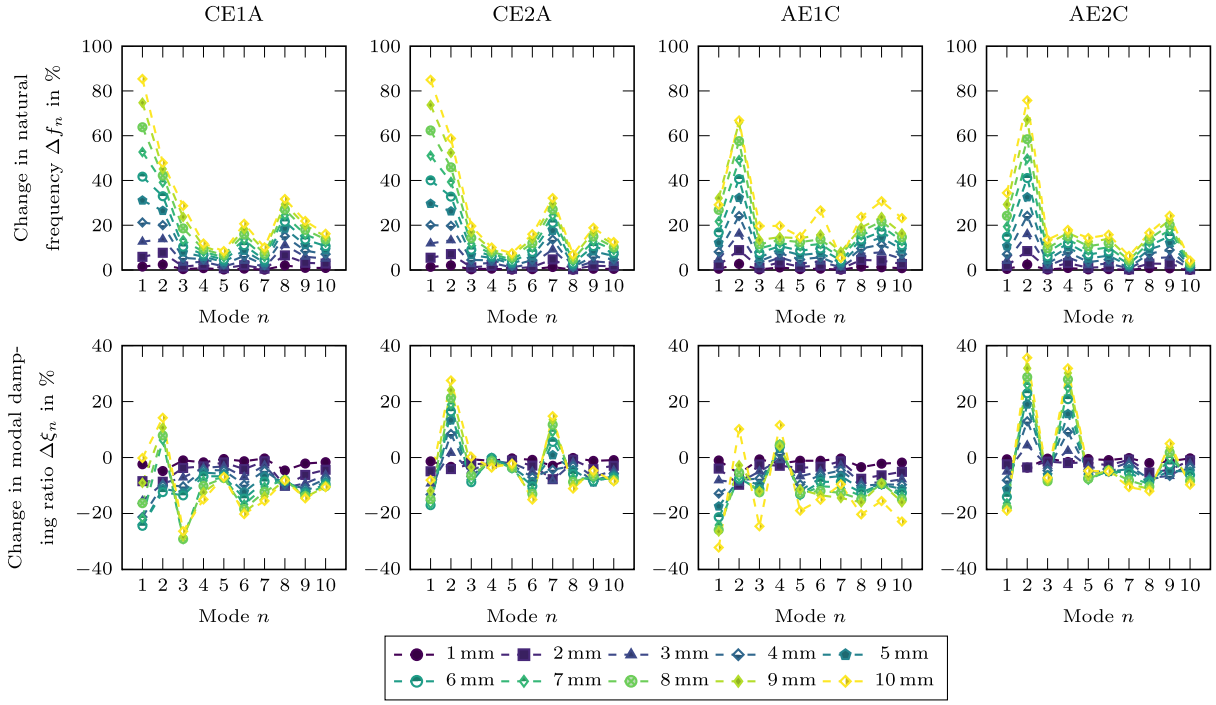

Fig. 15. Relative change in natural frequencies and modal damping ratios of the vibration modes listed in Table 5 compared to an undamaged plate (Fig. 8). Results are displayed for four different HyCEML configurations and different values of maximum predeformation depth w_{max} in Equation (6).

ample, Mode 2 exhibits significantly higher modal damping for higher values of w_{max}. Notably, higher values of w_{max} do not necessarily coincide with a greater change in modal damping ratio, as can be seen for Mode 1 in laminates CE1A and CE2A. Noteworthy is also the fact that for laminate CE2A, Mode 7 shows a decrease in modal damping for lower levels of predeformation, whereas increased modal damping ratios are observed for values of w_{max} exceeding 5 mm. In Modes 2 and 4 of laminate AE1C, very high values of w_{max} lead to an increase in modal damping, whereas lower values yield a decrease. In case of laminate AE2C, Mode 2 and Mode 4 also show an increase in modal damping, even for lower levels of predeformation.

The median changes of natural frequencies and modal damping ratios for permanently deformed plates are shown as box plots in Fig. 16 for different values of w_{max}. Median changes in natural frequencies adhere to an approximately linear correlation with the parameter w_{max}. Solely a deformation of $w_{max} = 10$ mm of laminate AE1C leads to a relatively higher median change in natural frequencies, which is explained by the nature of the median used here. Modes 6 and 9 are shifted overproportionally for $w_{max} = 10$ mm, as seen in Fig. 15, leading to a higher median change. For the median change of modal damping ratios, no such clear linear trend is visible, although the median change is consistently negative and increases with higher levels of predeformation in most cases. Upon comparison of the median changes in modal damping ratios, a similarity between laminates containing the same elastomer material is evident. Laminates CE1A and AE1C, featuring the softer elastomer, show a higher median decrease in modal damping ratios at given levels of permanent deformation. Laminates CE2A and AE2C on the other hand are less affected in their modal damping capabilities by the predeformation. Furthermore, higher values of w_{max} exceeding 8 mm seem to reduce the median decrease in modal damping ratios. The choice of elastomeric damping material, in this case, appears to have a higher influence on the damage tolerance of the CLD mechanism than the general laminate layup of HyCEMLs. The median changes in natural frequencies and modal damping ratios caused by permanent deformation exceed those caused by the other two types of damage. In their work, Li et al. [39] also attribute changes in vibrational behavior of FMELs mostly to permanent deformation and indentation of specimens.

4. Conclusions

This work investigates the damage tolerance of fiber-metal-elastomer laminates on the example of hybrid CFRP-elastomer-metal laminates with particular focus on the influence on their damping behavior. Experimental low-velocity impact tests show that the predominant types of damage inflicted into the laminate are intra-ply damage within the FRP plies, delaminations and permanent deformation. Following a numerical modal analysis study on damaged laminates, the following conclusions are obtained:

- Depending on the laminate layup and vibration mode, intra-ply damage of CFRP plies can either increase or decrease modal damping ratios. Laminates with CFRP plies on the outside show lower modal damping ratios when damaged by intra-ply damage, whereas laminates with aluminum on the outside see an increase in modal damping when damaged. Fiber damage has the predominant influence on natural frequencies as well as modal damping ratios compared to matrix damage. The choice of elastomer material determines the damage tolerance of modal damping towards intra-ply damage, depending on the type of laminate.
- Delaminations can lead to additional superimposed opening modes, which lead to a significant decrease in modal damping when adjacent to elastomer layers. However, delaminations can also cause an increase in modal damping, especially for stiffer elastomer damping layers. Delaminations taking up no more than 10% of the interface usually do not have a significant influence on the CLD mechanism.
- Permanent deformation after impact has the greatest influence on natural frequencies and modal damping ratios. While permanent deformation always leads to an increase in natural frequency due to a stiffening effect, some vibration modes also show an increase in modal damping. Consequently, laminates which deform less plastically, such as laminates of type CEA in this study, can be considered more damage tolerant with regard to their damping capabilities.

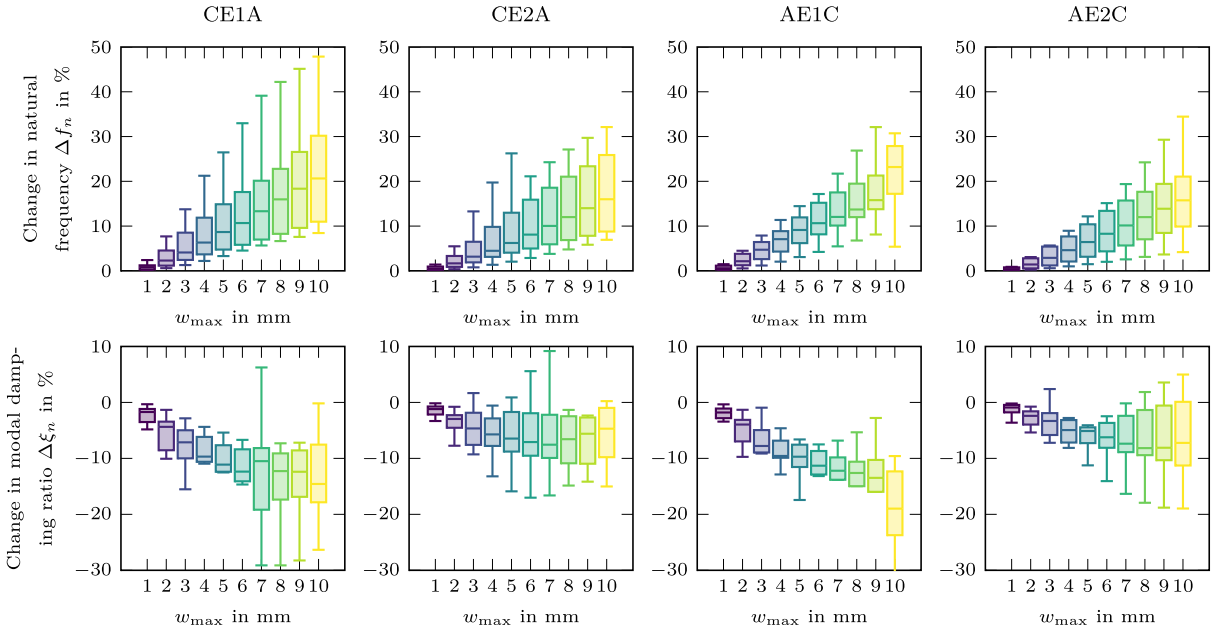

Fig. 16. Box plots showing the change of natural frequency and modal damping ratio of the first ten vibration modes caused by different levels of predeformation expressed by the maximum deformation depth w_{max} in Equation (6). Plots show the median values, the lower and upper quartiles as boxes and the minimum and maximum change values as whiskers.

It should be noted that most correlations identified in this work show a strong mode-dependency and that the specific influence of damage needs to be determined in a case-specific manner. Generally, these investigations show that the CLD mechanism in HyCEMLs is influenced by low-velocity impact damage, with damaged laminates even gaining modal damping capabilities in some cases.

CRediT authorship contribution statement

Alexander Jackstadt: Investigation, Methodology, Software, Visualization, Writing – original draft, Conceptualization. **Wilfried V. Liebig:** Supervision, Writing – review & editing. **Kay A. Weidenmann:** Funding acquisition, Supervision, Writing – review & editing. **Luise Kärger:** Funding acquisition, Supervision, Writing – review & editing.

Declaration of competing interest

The authors declare that they have no known competing financial interests or personal relationships that could have appeared to influence the work reported in this paper.

Data availability

The raw/processed data required to reproduce these findings cannot be shared at this time as the data also forms part of an ongoing study.

Acknowledgements

This work has been funded by the Deutsche Forschungsgemeinschaft (DFG, German Research Foundation) within the SPP1897 “Calm, Smooth, Smart – Novel approaches for influencing vibrations by means of deliberately introduced dissipation”, projects KA 4224/3-2 and WE 4273/16-2 “HyCEML – Hybrid CFRP/elastomer/metal laminates containing elastomeric interfaces for deliberate dissipation” (Karlsruhe Institute of Technology). The work is also part of the Heisenberg project “Digitalization of fiber-reinforced polymer processes for resource-efficient manufacturing of lightweight components”, funded by the DFG (project no. 798455807141). Furthermore, the authors would like to acknowledge Gummiwerk KRAIBURG GmbH & Co. KG for providing the elastomer material. Special gratitude is given to Vincent Sessner for manufacturing the specimens used in this work.

Appendix A. Forced vibration

Fig. A.17 shows a simply supported laminated plate of type AE2C under forced vibration. The delaminated plate shows additional peaks in the response curve when compared to the undamaged laminate, which can be attributed to additional opening modes of the delaminated area.

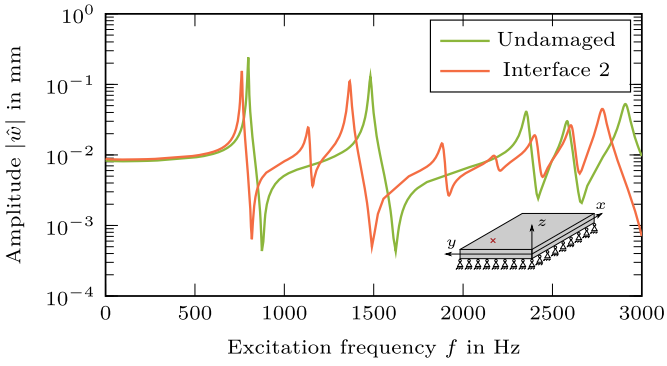

Fig. A.17. Numerically determined frequency response of simply supported laminates AE2C to forced vibration. Comparison of an undamaged laminate and one with a delamination in Interface 2. Response recorded at $x = 0.2a$ and $y = 0.2b$.

References

[1] T. Sinmazçelik, E. Avcu, M.Ö. Bora, O. Çoban, A review: fibre metal laminates, background, bonding types and applied test methods, Mater. Des. 32 (7) (2011) 3671–3685, https://doi.org/10.1016/j.matdes.2011.03.011.

[2] M. Sadighi, R.C. Alderliesten, R. Benedictus, Impact resistance of fiber-metal laminates: a review, Int. J. Impact Eng. 49 (2012) 77–90, https://doi.org/10.1016/j.ijimpeng.2012.05.006.

[3] J. Bienias, P. Jakubczak, K. Dadej, Low-velocity impact resistance of aluminium glass laminates – experimental and numerical investigation, Compos. Struct. 152 (15) (2016) 339–348, https://doi.org/10.1016/j.compstruct.2016.05.056.

[4] M. Stoll, F. Stemmer, S. Ilinzeer, K.A. Weidenmann, Optimization of corrosive properties of carbon fiber reinforced aluminum laminates due to integration of an elastomer interlayer, Key Eng. Mater. 742 (2017) 287–293, https://doi.org/10.4028/www.scientific.net/KEM.742.287.
[5] V. Sessner, M. Stoll, A. Feuvrier, K.A. Weidenmann, Determination of the damping characteristics of fiber-metal-elastomer laminates using piezo-indicated-loss-factor experiments, Key Eng. Mater. 742 (2017) 325–332, https://doi.org/10.4028/www.scientific.net/KEM.742.325.
[6] H. Oberst, Über die Dämpfung der Biegeschwingungen dünner Bleche durch fest haftende Beläge, Acta Acust. Acust. 2 (4) (1952) 181–194.
[7] V. Sessner, A. Jackstadt, W.V. Liebig, L. Kärger, K.A. Weidenmann, Damping characterization of hybrid carbon fiber elastomer metal laminates using experimental and numerical dynamic mechanical analysis, J. Compos. Sci. 3 (1) (2019) 3, https://doi.org/10.3390/jcs3010003.
[8] V. Sessner, W.V. Liebig, K.A. Weidenmann, Modal damping behavior of plane and 3D curved constrained layer damping CFRP-elastomer-metal laminates, Compos. Part C, Open Access 2 (2020) 100037, https://doi.org/10.1016/j.jcomc.2020.100037.
[9] V. Sessner, W.V. Liebig, A. Jackstadt, D. Schmid, T. Ehrig, K. Holeczek, N. Gräbner, P. Kostka, U. von Wagner, K.A. Weidenmann, L. Kärger, Wide scale characterization and modeling of the vibration and damping behavior of CFRP-elastomer-metal laminates—comparison and discussion of different test setups, Appl. Compos. Mater. 28 (5) (2021) 1715–1746, https://doi.org/10.1007/s10443-021-09934-7.
[10] Z. Li, J. Zhang, A. Jackstadt, L. Kärger, Low-velocity impact behavior of hybrid CFRP-elastomer-metal laminates in comparison with conventional fiber-metal laminates, Compos. Struct. 287 (7) (2022) 115340, https://doi.org/10.1016/j.compstruct.2022.115340.
[11] D. Düring, E. Petersen, D. Stefaniak, C. Hühne, Damage resistance and low-velocity impact behaviour of hybrid composite laminates with multiple thin steel and elastomer layers, Compos. Struct. 238 (5) (2020) 111851, https://doi.org/10.1016/j.compstruct.2019.111851.
[12] M.A. Zarezadeh-Mehrizi, G. Liaghat, H. Ahmadi, A. Taherzadeh-Fard, A. Khodadadi, Numerical and experimental investigation of fiber metal laminates with elastomeric layers under low–velocity impact, Polym. Compos. 43 (4) (2022) 1936–1947, https://doi.org/10.1002/pc.26509.
[13] V. Mahesh, Comparative study on low velocity impact response of carbon-fiber-reinforced polymer/thermoplastic elastomer based fiber metal laminates with and without interleaving of elastomeric layer, J. Thermoplast. Compos. Mater. (2023) 10.1177/08927057231180487.
[14] W. He, L. Wang, H. Liu, C. Wang, L. Yao, Q. Li, G. Sun, On impact behavior of fiber metal laminate (FML) structures: a state-of-the-art review, Thin-Walled Struct. 167 (2021) 108026, https://doi.org/10.1016/j.tws.2021.108026.
[15] E. Sarlin, M. Apostol, M. Lindroos, V.-T. Kuokkala, J. Vuorinen, T. Lepistö, M. Vippola, Impact properties of novel corrosion resistant hybrid structures, Compos. Struct. 108 (1) (2014) 886–893, https://doi.org/10.1016/j.compstruct.2013.10.023.
[16] E. Sarlin, M. Lindroos, M. Apostol, V.-T. Kuokkala, J. Vuorinen, T. Lepistö, M. Vippola, The effect of test parameters on the impact resistance of a stainless steel/rubber/composite hybrid structure, Compos. Struct. 113 (2014) 469–475, https://doi.org/10.1016/j.compstruct.2014.03.049.
[17] D. Düring, L. Weiß, D. Stefaniak, N. Jordan, C. Hühne, Low-velocity impact response of composite laminates with steel and elastomer protective layer, Compos. Struct. 134 (1110) (2015) 18–26, https://doi.org/10.1016/j.compstruct.2015.08.001.
[18] W.V. Liebig, V. Sessner, K.A. Weidenmann, L. Kärger, Numerical and experimental investigations of the damping behaviour of hybrid CFRP-elastomer-metal laminates, Compos. Struct. 202 (7) (2018) 1109–1113, https://doi.org/10.1016/j.compstruct.2018.05.051.
[19] A. Jackstadt, W.V. Liebig, V. Sessner, K.A. Weidenmann, L. Kärger, Application of a mixed variational higher order plate theory towards understanding the deformation behavior of hybrid laminates, PAMM 19 (1) (2019), https://doi.org/10.1002/pamm.201900048.
[20] A. Jackstadt, L. Kärger, Extension of an analytical solution of a unified formulation to the frequency response of composite plates with viscoelastic layers, PAMM 20 (1) (2021), https://doi.org/10.1002/pamm.202000234.
[21] A. Jackstadt, W.V. Liebig, L. Kärger, Analytical modeling and investigation of constrained layer damping in hybrid laminates based on a unified plate formulation, Int. J. Mech. Sci. 216 (2022) 106964, https://doi.org/10.1016/j.ijmecsci.2021.106964.
[22] R.L. Ramkumar, S.V. Kulkarni, R.B. Pipes, Free Vibration Frequencies of a Delaminated Beam, Proceedings of the 34th Annual Technical Conference, vol. 22-E, Society of the Plastics Industry, 1979, pp. 1–5.
[23] J.T.S. Wang, Y.Y. Liu, J.A. Gibby, Vibrations of split beams, J. Sound Vib. 84 (4) (1982) 491–502, https://doi.org/10.1016/S0022-460X(82)80030-8.
[24] P.M. Mujumdar, S. Suryanarayan, Flexural vibrations of beams with delaminations, J. Sound Vib. 125 (3) (1988) 441–461, https://doi.org/10.1016/0022-460X(88)90253-2.
[25] M.-H.H. Shen, J.E. Grady, Free vibrations of delaminated beams, AIAA J. 30 (5) (1992) 1361–1370, https://doi.org/10.2514/3.11072.
[26] C.N. Della, D. Shu, Vibration of delaminated multilayer beams, Composites, Part B, Eng. 37 (2–3) (2005) 227–236, https://doi.org/10.1016/j.compositesb.2005.05.006.
[27] G.S. Ramtekkar, Free vibration analysis of delaminated beams using mixed finite element model, J. Sound Vib. 328 (4–5) (2009) 428–440, https://doi.org/10.1016/j.jsv.2009.08.008.
[28] Z. Zhang, K. Shankar, M. Tahtali, E.V. Morozov, Vibration modelling of composite laminates with delamination damage, in: M. Burgess (Ed.), 20th International Congress on Acoustics 2010, 2010, pp. 1–8, printed by Curran Associates, Red Hook, N.Y.
[29] Y. Liu, J. Xiao, D. Shu, Free vibration of exponential functionally graded beams with single delamination, Proc. Eng. 75 (2014) 164–168, https://doi.org/10.1016/j.proeng.2013.11.041.
[30] X. Li, D. Halim, Free and forced vibration modelling of a delaminated beam structure using a Green's function method, Acta Mech. 234 (7) (2023) 2889–2906, https://doi.org/10.1007/s00707-023-03527-0.
[31] H. Luo, S. Hanagud, Dynamics of delaminated beams, Int. J. Solids Struct. 37 (10) (2000) 1501–1519, https://doi.org/10.1016/S0020-7683(98)00325-4.
[32] R.-A. Jafari-Talookolaei, M. Abedi, M. Hajianmaleki, Vibration characteristics of generally laminated composite curved beams with single through-the-width delamination, Compos. Struct. 138 (2016) 172–183, https://doi.org/10.1016/j.compstruct.2015.11.050.
[33] C.N. Della, D. Shu, Vibration of delaminated composite laminates: a review, Appl. Mech. Rev. 60 (1) (2007) 1–20, https://doi.org/10.1115/1.2375141.
[34] W.-L. Yin, K.C. Jane, Vibration of a delaminated beam-plate relative to buckled states, J. Sound Vib. 156 (1) (1992) 125–140, https://doi.org/10.1016/0022-460X(92)90816-G.
[35] H.-P. Chen, Free vibration of prebuckled and postbuckled plates with delamination, Compos. Sci. Technol. 51 (3) (1994) 451–462, https://doi.org/10.1016/0266-3538(94)90113-9.
[36] S. Dey, A. Karmakar, Free vibration analyses of multiple delaminated angle-ply composite conical shells – a finite element approach, Compos. Struct. 94 (7) (2012) 2188–2196, https://doi.org/10.1016/j.compstruct.2012.01.006.
[37] S. Ganesh, K.S. Kumar, P.K. Mahato, Free vibration analysis of delaminated composite plates using finite element method, Proc. Eng. 144 (2016) 1067–1075, https://doi.org/10.1016/j.proeng.2016.05.061.
[38] Z.-X. Wang, P. Qiao, J. Xu, Vibration analysis of laminated composite plates with damage using the perturbation method, Composites, Part B, Eng. 72 (2015) 160–174, https://doi.org/10.1016/j.compositesb.2014.12.005.
[39] H. Li, Z. Li, Z. Xiao, X. Wang, J. Xiong, J. Zhou, Z. Guan, Development of an integrated model for prediction of impact and vibration response of hybrid fiber metal laminates with a viscoelastic layer, Int. J. Mech. Sci. 197 (3) (2021) 106298, https://doi.org/10.1016/j.ijmecsci.2021.106298.
[40] V. Sessner, W.V. Liebig, L. Kärger, K.A. Weidenmann, Experimental and numerical characterisation of fibre–metal–elastomer laminates by using DMA regarding its damping behaviour, PAMM 18 (1) (2018), https://doi.org/10.1002/pamm.201800432.
[41] Gummiwerk KRAIBURG GmbH & Co. KG, Technical Data Sheet KRAIBON® SAA9579/52, 2014.
[42] Gummiwerk KRAIBURG GmbH & Co. KG, Technical data sheet KRAIBON® HAA9275/45, 2022.
[43] I. Lapczyk, J.A. Hurtado, Progressive damage modeling in fiber-reinforced materials, Composites, Part A, Appl. Sci. Manuf. 38 (11) (2007) 2333–2341, https://doi.org/10.1016/j.compositesa.2007.01.017.
[44] A.P. Sharma, S.H. Khan, R. Kitey, V. Parameswaran, Effect of through thickness metal layer distribution on the low velocity impact response of fiber metal laminates, Polym. Test. 65 (2018) 301–312, https://doi.org/10.1016/j.polymertesting.2017.12.001.
[45] L. Mullins, Effect of stretching on the properties of rubber, Rubber Chem. Technol. 21 (2) (1948) 281–300, https://doi.org/10.5254/1.3546914.
[46] A. Jackstadt, F. Frölich, K.A. Weidenmann, L. Kärger, Modeling the Mullins effect of rubbers used in constrained–layer damping applications, PAMM 21 (1) (2021), https://doi.org/10.1002/pamm.202100098.
[47] M. Gröhlich, A. Lang, M. Böswald, J. Meier, Viscoelastic damping design – thermal impact on a constrained layer damping treatment, Mater. Des. 207 (7) (2021) 109885, https://doi.org/10.1016/j.matdes.2021.109885.